PHYSICAL REVIEW B **89**, 201101(R) (2014)

Spectroscopic evidence for exceptionally high orbital moment induced by local distortions in α-CoV_2O_6

N. Hollmann,[1] S. Agrestini,[1] Z. Hu,[1] Z. He,[2] M. Schmidt,[1] C.-Y. Kuo,[1] M. Rotter,[1] A. A. Nugroho,[3] V. Sessi,[4] A. Tanaka,[5] N. B. Brookes,[4] and L. H. Tjeng[1]

[1]*Max-Planck-Institut für Chemische Physik fester Stoffe, Nöthnitzer Str. 40, 01187 Dresden, Germany*

[2]*State Key Laboratory of Structural Chemistry, Fujian Institute of Research on the Structure of Matter, Chinese Academy of Sciences, Fuzhou, Fujian 350002, China*

[3]*Faculty of Mathematics and Natural Sciences, Institut Teknologi Bandung, Jl. Ganesha 10, Bandung 40132, Indonesia*

[4]*European Synchrotron Radiation Facility, CS40220, F-38043 Grenoble Cedex 9, France*

[5]*Department of Quantum Matter, ADSM, Hiroshima University, Higashi-Hiroshima 739-8530, Japan*

(Received 25 July 2013; revised manuscript received 31 March 2014; published 2 May 2014)

We present a combined experimental and theoretical study on the local magnetism of the Co ions in the spin-chain compound CoV_2O_6, which crystallizes in two different allotropic phases, α- and γ-CoV_2O_6. Using x-ray magnetic circular dichroism, we have found an exceptionally high and a moderate orbital contribution to the magnetism in α-CoV_2O_6 and γ-CoV_2O_6, respectively. Full-multiplet calculations indicate that the differences in the magnetic behavior of α- and γ-CoV_2O_6 phases originate from different local distortions of the CoO_6 octahedra. In particular, the strong compression of the CoO_6 octahedra together with the unusually small octahedral crystal field splitting in α-CoV_2O_6 lead to a strong mixture of t_{2g} and e_g orbitals which, via the local atomic Coulomb and exchange interactions, results in an exceptionally large orbital moment.

DOI: 10.1103/PhysRevB.89.201101 PACS number(s): 71.70.Ej, 71.70.Ch, 78.70.Dm, 72.80.Ga

Low-dimensional magnetic spin systems have attracted high interest in solid state physics due to their complex magnetic behavior. Magnetic ions in these materials are arranged in, e.g., planes, ladders, or linear chains. The low-dimensional magnetic sublattice may lead to a rich phase diagram, where small changes in magnetic field and temperature induce a rearrangement of the magnetic order. An example is $Ca_3Co_2O_6$, in which chains of Co^{3+} ions are arranged on a triangular lattice with a steplike magnetization in the ordered state [1–4]. X-ray magnetic dichroism experiments and theoretical work provided detailed information on the orbital occupation, the charge and spin state, as well as the orbital moment explaining the magnetic anisotropy in $Ca_3Co_2O_6$ [5,6].

Recently, a new spin-chain compound CoV_2O_6 was synthesized [7]. The compound crystallizes in two different allotropic phases, monoclinic α-CoV_2O_6 (space group $C2/m$, $a = 9.289$ Å, $b = 3.535$ Å, $c = 6.763$ Å, $\beta = 112.64°$) and triclinic γ-CoV_2O_6 (space group $P\bar{1}$, $a = 7.164$ Å, $b = 8.872$ Å, $c = 4.806$ Å, $\alpha = 90.29°$, $\beta = 93.66°$, $\gamma = 102.05°$) [8–10]. In both structures, edge-sharing CoO_6 octahedra form chains running along the b axis. The CoO_6 chains are separated by zigzag chains made of VO_5 pyramids and VO_6 octahedra for the monoclinic and the triclinic structure, respectively. The V ions are in a nonmagnetic V^{5+} ($3d^0$) state and the magnetic properties are determined by the Co^{2+} ions. A steplike behavior is found in the isothermal magnetization curves in the ordered state, both for α- and γ-CoV_2O_6 [7,11–13]. The saturation magnetizations of the two phases, however, are quite different: 4.5 μ_B and 2.9 μ_B per Co ion for the α and γ phases, respectively. Presupposing a spin moment of 3 μ_B for Co^{2+} ($S = 3/2$), the magnetism for α-CoV_2O_6 must have a large orbital contribution. Kim *et al.* [14] have used density functional theory (DFT) to estimate the orbital moment of both phases. The difference in the magnetic properties between the two phases is attributed to the different local distortion of the CoO_6 octahedra. GGA+spin-orbit coupling (SO) approximation, however, underestimates the orbital moment for the α phase. In order to reproduce the experimental moment, it is necessary to include an orbital polarization (OP) term yielding an orbital moment of 1.8 μ_B with a large uniaxial anisotropy along the c axis. The orbital occupation was given in terms of complex orbitals $d_{\pm2}$, $d_{\pm1}$, and d_0 in analogy to $Ca_3Co_2O_6$. For this compound, one minority electron occupies the $d_{\pm2}$ orbitals giving an orbital moment close to 2 μ_B [5,6]. In case that $d_{\pm2}$, $d_{\pm1}$, and d_0 are indeed eigenstates for α-CoV_2O_6, the orbital moment could be even 3 μ_B.

However, the local coordination of Co in α-CoV_2O_6 is different from that in $Ca_3Co_2O_6$: the magnetic high spin Co^{3+} ion in $Ca_3Co_2O_6$ has a trigonal prismatic local symmetry, while α-CoV_2O_6 contains distorted octahedra exhibiting a different ligand field level scheme. This requires in our opinion a different quantitative explanation of the local magnetic properties. In fact, there are more reasons why $Ca_3Co_2O_6$ should not be considered an analog of CoV_2O_6. The latter contains only divalent Co as magnetic ion, while the former has high spin Co^{3+} as magnetic ion and additional low spin Co^{3+} ($3d^6$) as nonmagnetic ion. In $Ca_3Co_2O_6$, the Co chains consist of alternating magnetic and nonmagnetic Co^{3+} ions with the easy axis pointing along the chain direction and the magnetic exchange coupling works indirectly over the oxygen ligands. In α-CoV_2O_6, the easy axis is perpendicular to the chain direction and magnetic exchange is realized by superexchange between the Co^{2+} ions in their edge-sharing octahedra.

Here, we report on our study of the local magnetism in both phases using x-ray magnetic circular dichroism (XMCD) spectroscopy at the Co-$L_{2,3}$ edge. The XMCD technique provides separate information on spin and orbital moments, and in addition the x-ray absorption spectroscopy (XAS) line

shape yields details on the local electronic structure and the ligand field splittings. We use a full-multiplet configuration-interaction approach to model the experimental spectra as well as the experimentally determined magnetic moments. We are able to track down quantitatively and qualitatively the essential ingredients for the anomalously large orbital moment in α-CoV_2O_6. Our results directly confirm that the orbital magnetism in α-CoV_2O_6 stems from the unusual local coordination, and that the large size of the moment needs a many-body description.

Single crystals of α-CoV_2O_6 have been grown by the flux method described in Ref. [7]. Single crystals of γ-CoV_2O_6 have been grown by starting from $CoC_2O_4{\cdot}2H_2O$ and V_2O_5. The stoichiometric mixture was heated in a corundum crucible in air up to 600 °C in 24 h and annealed at this temperature for 92 h. The crystals of γ-CoV_2O_6 were obtained by chemical vapour transport. The transport process was carried out from a microcrystalline sample of γ-CoV_2O_6 in an evacuated quarz tube in a temperature gradient from 730 °C (source) to 630 °C (sink). $TeCl_4$ (2.5 mg/ml) was used as transport agent. The XAS experiments were performed at the ID08 beamline of the ESRF synchrotron facility in Grenoble, France. The crystals were cleaved *in situ* in ultrahigh vacuum in the low 10^{-10} mbar range to obtain clean sample surfaces. A fast-switchable high-field magnet was used to obtain the XMCD signal at the Co-$L_{2,3}$ edge. The energy resolution was ≈0.25 eV with a degree of circular polarization of larger than 99%. The magnetic field direction was chosen parallel to the c axis for α-CoV_2O_6, which is the direction where the steplike behavior is observed in the magnetization measurements [7]. We used a field of $B = 5$ T at 10 K, so that approximately 90% of the saturation magnetization is picked up, according to the magnetization curves in Ref. [15]. The magnetic field was parallel to the b axis for γ-CoV_2O_6. A CoO sample was measured simultaneously and used as reference. The absorption spectra were obtained in total electron yield mode and the minor self-absorption effects were corrected using the procedure given by Nakajima *et al.* [16]. DFT calculations have been performed with the FPLO code [17] for α- and γ-CoV_2O_6, using the experimental crystal structures [10,18]. We have chosen the LDA approximation [19] and calculated the density of states on a mesh of $24 \times 24 \times 24$ k points.

We first discuss the experimental XAS of γ-CoV_2O_6 depicted in Fig. 1. The $L_{2,3}$ edge shows the dipole-allowed $2p^6 3d^n \rightarrow 2p^5 3d^{n+1}$ transition, which is highly sensitive to the electronic ground state of the $3d$ shell in terms of valence and the local coordination [20]. The line shape and the energy position of γ-CoV_2O_6 spectrum clearly indicate that the charge state is Co^{2+}. The XAS line shape of γ-CoV_2O_6 is very similar to that of CoO or $LaMn_{0.5}Co_{0.5}O_3$ compounds which have Co ions in an almost regular octahedral environment [21]. The XMCD signal, being sensitive to both magnitude and sign of the spin and orbital contributions to the magnetic moment, resembles the one of $LaMn_{0.5}Co_{0.5}O_3$ [21] in line shape and opposite sign at the L_3 and L_2 lines, indicating similar local magnetic properties, including a moderate value of the orbital moment of about 1 μ_B. For a quantitative analysis, we first utilize the sum rules in XMCD [22]. For the ratio of orbital and spin moments, when the magnetic quadrupole moment T_z

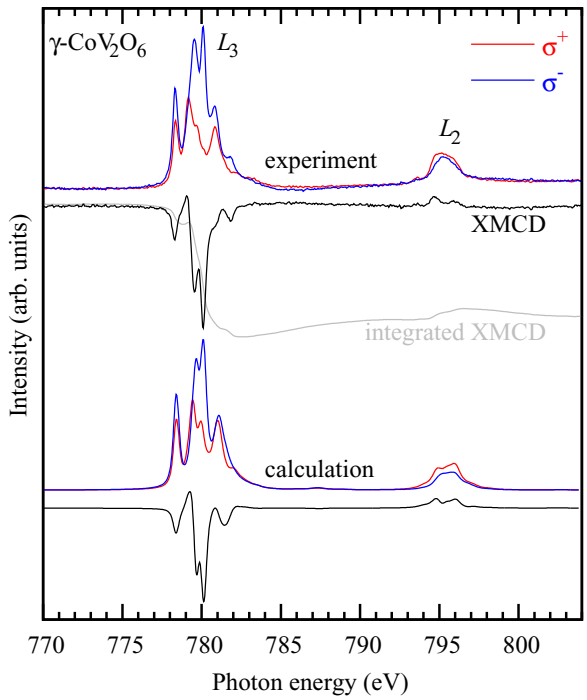

FIG. 1. (Color online) Co-$L_{2,3}$ edge x-ray magnetic circular dichroism for γ-CoV_2O_6.

is ignored [23], the sum rules can be expressed as [24]

$$\frac{m_{\mathrm{orb}}}{m_{\mathrm{spin}}} = \frac{2}{3}\frac{\int_{L_{2,3}}(\sigma^+ - \sigma^-)dE}{\int_{L_3}(\sigma^+ - \sigma^-)dE - 2\int_{L_2}(\sigma^+ - \sigma^-)dE}. \quad (1)$$

The advantage of this sum rule is that the desired values for spin and orbital moments can be extracted directly from the XMCD spectrum without the need to subtract a step-edge background. For γ-CoV_2O_6, it yields $m_{\mathrm{orb}}/m_{\mathrm{spin}} \approx 0.49$.

The XAS of α-CoV_2O_6 in Fig. 2 also shows a high spin Co^{2+} state. The line shape of σ^+, σ^-, and the XMCD spectra, however, are very different from those of γ-CoV_2O_6. The most striking feature is the same negative sign of the XMCD signal at the L_3 and L_2 lines. This is quite unusual for a solid, as the sign of the XMCD signal is typically opposite at the L_3 and L_2 lines reflecting a reduction of orbital moment of the transition metal ions in the solid state from its atomic value. The negative signs of the XMCD signal in α-CoV_2O_6 are in that sense indicating that the Co ions in α-CoV_2O_6 may effectively have free-ion like quantum numbers in its ground state [25]. Using the sum rule (1), $m_{\mathrm{orb}}/m_{\mathrm{spin}} \approx 0.73$ is found, which is clearly larger than the value for γ-CoV_2O_6.

As the Co-$L_{2,3}$ XAS line shape contains signatures of the microscopic origin of the exceptionally high orbital moment in α-CoV_2O_6, and the large difference compared to γ-CoV_2O_6, we make a further analysis by carrying out simulations of the spectra using the well-proven full-multiplet configuration-interaction approach [20,26]. The calculations were performed using the XTLS 9.0 code [27]. This type of calculation has the advantage of taking the spin-orbit coupling explicitly into account in exact diagonalization. The monopole parts of the Coulomb interaction as well as the charge-transfer energy [28] were taken from CoO [29]. Covalence between

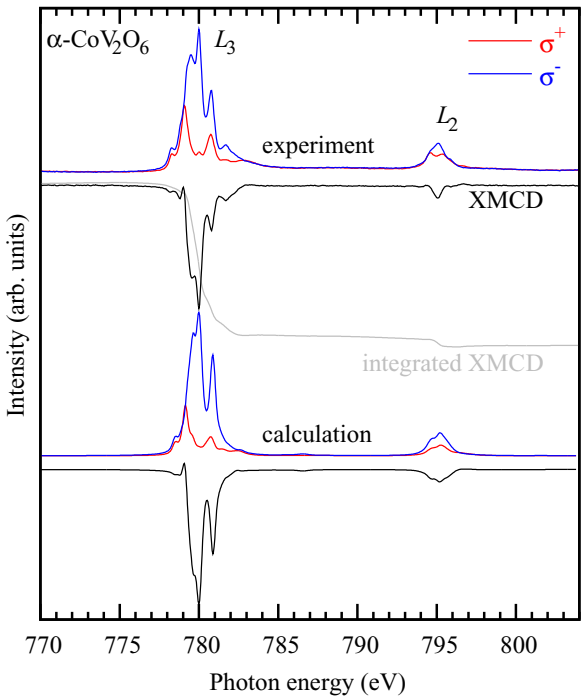

FIG. 2. (Color online) Co-$L_{2,3}$ edge x-ray magnetic circular dichroism for α-CoV_2O_6.

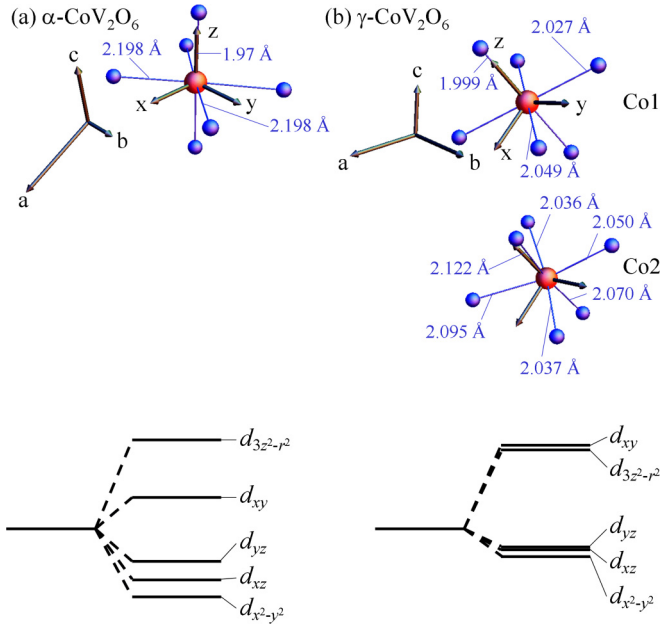

FIG. 3. (Color online) Local coordination of the Co ions with Co-O bond lengths. The schematic ligand field splittings are given below, omitting the small mixing between $d_{x^2-y^2}$ and $d_{3z^2-r^2}$ orbitals.

Co and O was taken into account using the formalism of Slater and Koster [30]. Hybridization strengths were calculated from Harrison's book [31] using the experimental Co-O bond lengths [10,18]. See also the local coordinate system as illustrated in Fig. 3. Note that the local x and y axes are pointing in between the Co-O bonds.

The parameters to be optimized are then the *ionic* one-electron crystal field splittings between the relevant $3d$ orbitals, which reflect the local coordination of the Co ions. The leading parameter here is the cubic splitting $10Dq$, which defines the energy difference between the lower t_{2g} (d_{yz}, d_{xz}, and $d_{x^2-y^2}$ orbitals) and higher e_g (d_{xy} and $d_{3z^2-r^2}$) levels. $10Dq$ roughly scales with the average Co-O bond length in the octahedron, with an increasing value for $10Dq$ for smaller bond lengths. The t_{2g} and e_g levels are further split when the local symmetry is lower than cubic as in the case of CoV_2O_6. For a compressed tetragonal distortion, the $d_{x^2-y^2}$ is lowered in respect to the d_{yz} and d_{xz} orbitals. We denote this energy difference as Δt_{2g} with a negative sign for compression. In the e_g levels, d_{xy} is lowered in respect to $d_{3z^2-r^2}$, which we denote with a negative energy difference Δe_g. An orthorhombic distortion will split d_{yz} and d_{xz} orbitals in energy and allow mixing of d_{xy} and $d_{x^2-y^2}$ characters.

As a first step, we tune the values for the ionic part of the crystal fields such that the resulting effective crystal fields or effective one-electron energy levels of the $3d$ orbitals (i.e., including the effect of the hybridization with the oxygens), are close to the estimates from *ab initio* band-structure calculations. We carried out DFT calculations for CoV_2O_6 in the nonmagnetic state using the FPLO code and obtained Co $3d$ partial density of states (PDOS) very similar to those of Kim *et al.* [14]. The first moments of the Co-$3d$-dominated PDOS yield effective crystal field values of $10Dq = 0.52$ eV, $\Delta t_{2g} = 0.06$ eV, and $\Delta e_g = -0.24$ eV for α-CoV_2O_6. It turned out that the simulated XAS and XMCD spectra do not provide an optimal match with the experimental ones. Also the orbital moment calculated using these parameters is about 1.1 μ_B, i.e., smaller than value deduced using the XMCD orbital sum rule on the α-CoV_2O_6 experimental spectra.

In the next step, we fine tune the crystal field values to obtain an optimal fit to the α-CoV_2O_6 experimental spectra. The effective crystal field values came out to be $10Dq = 0.52$ eV, $\Delta t_{2g} = -0.21$ eV, and $\Delta e_g = -0.60$ eV and a sketch of the effective one-electron energy levels is displayed in Fig. 3. Here, in contrast to the result from DFT, the sign of the crystal field splittings are in accordance to the local coordination, as a compression along z should lower the energy of the orbitals that are in the xy plane, i.e., the d_{xy} and $d_{x^2-y^2}$ orbitals should be lower in e_g and t_{2g} levels, respectively. The eigenstates of the many-body calculation including spin-orbit coupling, however, are a mixture of the eigenstates of the crystal field (d_{yz}, d_{xz}, $d_{x^2-y^2}$, d_{xy}, and $d_{3z^2-r^2}$) and spin-orbit coupling (d_0, $d_{\pm1}$, and $d_{\pm2}$). The resulting simulations are shown in Fig. 2. One can clearly see that these simulations reproduce all the experimental σ^+, σ^-, and XMCD spectra very well. Our cluster calculations show that the first excited state for the Co^{2+} ion is 39.4 meV higher in energy than the ground state. With the experiment carried out at 10 K, we therefore can confirm that we are probing the ground state properties of the system. The orbital moment calculated using these parameter set is $m_{\text{orb}} = 1.9\ \mu_B$. The calculated spin moment is $m_{\text{spin}} = 2.5\ \mu_B$, giving a total magnetic moment of 4.4 μ_B for the α phase, i.e., reproducing excellently the saturation magnetization value [7,12], and in good agreement with the result from the sum rule given above. This exceptionally high orbital moment and the spin-orbit coupling lead to a strong magnetocrystalline anisotropy (2.3 meV from our multiplet

calculations) with the magnetic moment aligned along the c axis. We note that these optimized effective crystal field values do not deviate very much in absolute terms from the above listed band structure estimates. Nevertheless, discrepancies of 0.27 eV in Δt_{2g} and 0.36 eV in Δe_g are very large compared to the Co $3d$ spin-orbit constant, implying that more accurate methods [32–34] need to be explored if one wishes to make estimates for the crystal fields on the basis of *ab initio* theories.

Another important note that we would like to make is that we have calculated not only the XAS and XMCD spectra using the full atomic multiplet theory (i.e., including all spin and orbital flip terms of the atomic Coulomb and exchange interactions), but also the orbital and spin moments. Instead, when we use a one-electron scheme [35], we will find an orbital moment of only $m_{\rm orb} = 1.0\ \mu_B$, i.e., substantially smaller than the $m_{\rm orb} = 1.9\ \mu_B$ value in the full multiplet approach (using the same one-electron energy levels). This may explain why Kim *et al.* [14] needed to include the orbital polarization term in their calculations to improve their DFT results.

The γ-CoV_2O_6 phase contains two different cobalt sites, see Fig. 3. Both sites are taken into account in the calculation. The crystal field splittings of the two sites are rather close, and we find in average $10Dq = 1.07$ eV, $\Delta t_{2g} = -0.02$ eV, and $\Delta e_g = 0.04$ eV as values for the effective crystal fields in order to reproduce the experimental XAS and XMCD spectra, see Fig. 1. The value of $10Dq = 1.07$ eV is, compared, for example, to the case of CoWO4 (0.9 eV) [36] and CoO (0.7 eV) [37], rather large, which is a result of the short average bond length of 2.047 Å in γ-CoV_2O_6. The moments calculated using these parameters are $m_{\rm orb} = 0.7\ \mu_B$ and $m_{\rm spin} = 1.8\ \mu_B$, giving a total moment of 2.5 μ_B, close to the results of the magnetization experiments [7,12]. It is clear that these effective crystal field values corresponds to an almost cubic local Co coordination, see the illustration in the right panel of Fig. 3.

Let us look into the details of the local environment of Co^{2+} to illustrate the reason for the exceptionally high orbital moment in α-CoV_2O_6 in a many-body picture. First, we regard cubic symmetry and ignore mixing of t_{2g} and e_g states. For high spin $3d^7$ with $t_{2g}^5 e_g^2$ occupation, the total spin of $S = 3/2$ couples with the pseudo-orbital momentum $\tilde{L} = 1$ to $\tilde{J} = 1/2$ as state lowest in energy. The orbital occupation for the hole within the t_{2g} states is somewhat similar to the case of t_{2g}^5 [38], with a combination of $d_{\pm1}$ and d_{xy} orbitals. Due to spin-orbit coupling, the eigenstates are not purely d_{+1} or d_{-1}; the resulting value for the orbital moment is $L_z = 2/3\ \mu_B$. In presence of a tetragonal distortion, depending on whether the octahedron is compressed or elongated, either the d_{xy} (b_{2g}) or the $d_{\pm1}$ (e_g) manifold is stabilized, leading to an increase or decrease of the orbital moment, respectively [18,29]. If only the t_{2g} states are considered, the value of L_z reaches up to 1 μ_B; this is the maximum that can be created by one hole occupation of the d_{+1} orbital in *compressed* distortion. Any in-plane orthorhombic distortion will reduce the orbital moment as it tends to stabilize the hole in one of the real orbitals d_{xy}, d_{xz}, or d_{yz}. To explain the exceptionally high L_z in α-CoV_2O_6, the e_g orbitals have to be taken into account [14]. The mixing of d_{xy} and $d_{x^2-y^2}$ orbitals brings $d_{\pm2}$ orbital character into the ground state and enhances the orbital moment. For a given spin-orbit coupling strength, the amount of the admixture depends on the type of the CoO_6 distortion, namely the energy splitting of the five $3d$ orbitals. There is an additional important difference in the energetics between the $d_{\pm1}$ and the $d_{\pm2}$ orbitals; the mixing matrix element due to spin-orbit coupling is twice as large for the $d_{\pm2}$ orbitals, an effect which is even squared for small energy separations.

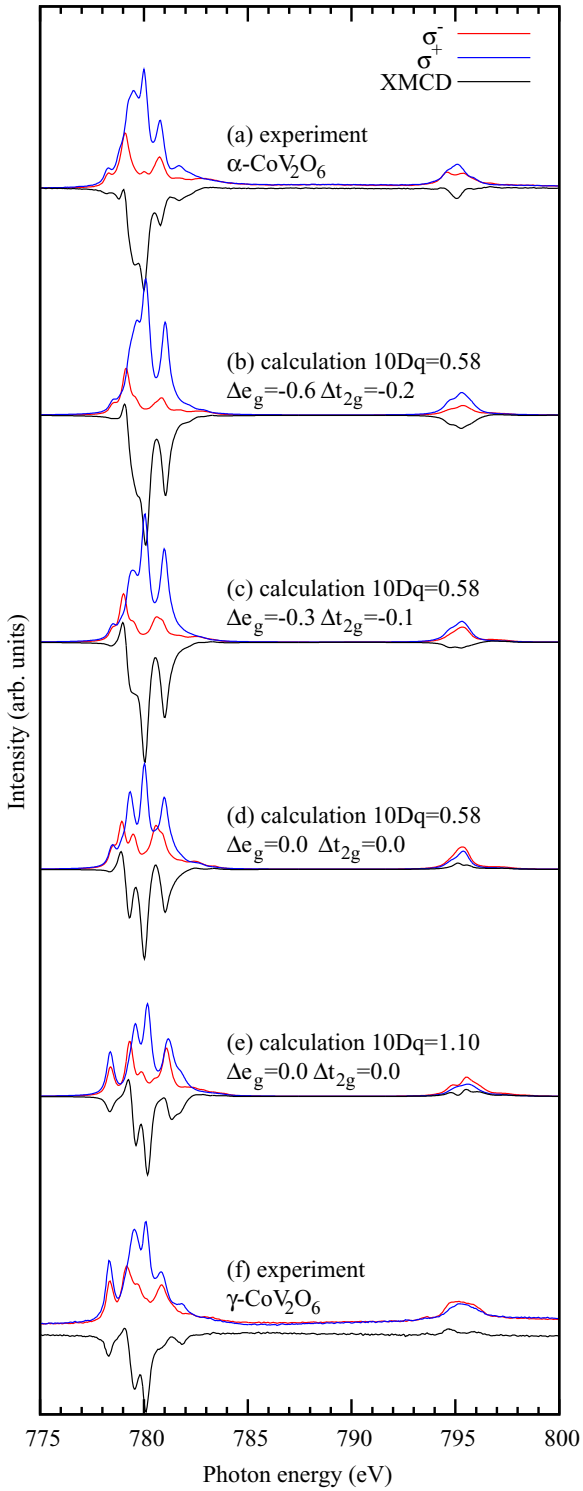

FIG. 4. (Color online) Influence of octahedral compression on the Co-$L_{2,3}$ edge x-ray magnetic circular dichroism. See text for the details on the calculations.

From this conjecture, we can conclude that for an enhancement of L_z from a cubic symmetry, the local coordination should have (1) a large compressed distortion to generate strong mixing terms between the e_g and t_{2g} orbitals, (2) a small $10Dq$ corresponding to large average bond lengths in order to bring the e_g close in energy to the t_{2g} orbitals, and (3) only small to moderate orthorhombic distortion in the xy plane of the octahedron to avoid the formation of real space orbitals.

Let us study a simplified model of the local environment to illustrate its effect on the spectra and the orbital moment. The experimental spectra are given in Figs. 4(a) and 4(f), for α-CoV_2O_6 and γ-CoV_2O_6, respectively. To obtain the calculated curves (b)–(e), we have performed ionic calculations and approximated the local environment as tetragonal: the crystal field is characterized by the cubic splitting $10Dq$ between e_g and t_{2g} levels; the levels are further split up by Δt_{2g} (lowering the $d_{x^2-y^2}$ orbital with respect to the d_{xz}/d_{yz} orbitals) and Δe_g (lowering the d_{xy} orbital with respect to the $d_{3z^2-r^2}$ orbital). First compare the spectra in Figs. 4(b)–4(d), where the cubic splitting $10Dq$ is held constant while the size of the splittings Δt_{2g} and Δe_g is reduced from (b) to (d). This resembles a thought experiment in which the average bond length of the CoO_6 octahedron is kept constant, while reducing the compression of the apical oxygen atoms. It can be seen in the spectra that the XMCD on the L_2 line reverses its sign between curves (c) and (d), which is evidence for the strong dependence of the orbital moment on the amount of compression; the increase of compression when going from (d) to (b) drastically increases the orbital moment. Comparing curve (b) to the experimental spectrum for α-CoV_2O_6 given in (a), it can be seen that the main features are already properly described in this simple model, and that the line shape of the XMCD reflects the local environment. In curves (d) and (e), the dependence of the spectrum on the cubic splitting $10Dq$ is demonstrated: the line shape of the spectral features for each polarization is changed, but the total integral of the XMCD, corresponding to the amount of orbital moment, is only slightly affected. Increasing the size of $10Dq$ leads to a better resemblance to the experimental spectrum of γ-CoV_2O_6, compare curves (e) and (f). The spectra in Fig. 4 demonstrate that indeed the leading term in the difference in the orbital moment between α- and γ-CoV_2O_6 is the amount of compression of the CoO_6 octahedra. For the spectral line-shape differences, also the magnitude of $10Dq$ matters.

To summarize, we have examined the local magnetism of the Co spin chain compounds α-CoV_2O_6 and γ-CoV_2O_6 experimentally with x-ray magnetic circular dichroism. We are able to confirm quantitatively that the exceptionally high orbital contribution to the magnetic moment for α-CoV_2O_6 is caused by the strong compression of the octahedra and by the fact that the octahedral crystal field splitting is unusually small. That the effect of the local symmetry is exceptionally large can be traced back to the multiplet nature of the atomic Coulomb and exchange interactions within the Co $3d$ shell.

We gratefully acknowledge the ESRF staff for providing beamtime. We thank B. Kim for fruitful discussions.

[1] S. Aasland, H. Fjellvåg, and B. Hauback, Solid State Commun. **101**, 187 (1997).
[2] H. Kageyama, K. Yoshimura, K. Kosuge, H. Mitamura, and T. Goto, J. Phys. Soc. Jpn. **66**, 1607 (1997).
[3] A. Maignan, C. Michel, A. Masset, C. Martin, and B. Raveau, Eur. Phys. J. B **15**, 657 (2000).
[4] V. Hardy, M. R. Lees, O. A. Petrenko, D. McK. Paul, D. Flahaut, S. Hebert, and A. Maignan, Phys. Rev. B **70**, 064424 (2004).
[5] T. Burnus, Z. Hu, M. W. Haverkort, J. C. Cezar, D. Flahaut, V. Hardy, A. Maignan, N. B. Brookes, A. Tanaka, H. H. Hsieh, H.-J. Lin, C. T. Chen, and L. H. Tjeng, Phys. Rev. B **74**, 245111 (2006).
[6] H. Wu, M. W. Haverkort, Z. Hu, D. I. Khomskii, and L. H. Tjeng, Phys. Rev. Lett. **95**, 186401 (2005).
[7] Z. He, J.-I. Yamaura, Y. Ueda, and W. Cheng, J. Am. Chem. Soc. **131**, 7554 (2009).
[8] B. Jasper-Tönnies and H. Müller-Buschbaum, Z. Anorg. Allg. Chem. **508**, 7 (1984).
[9] K. Mocała, J. Ziołkowski, and L. Dziembaj, J. Solid State Chem. **56**, 84 (1985).
[10] H. Müller-Buschbaum and M. Kobel, J. Alloys Compounds **176**, 39 (1991).
[11] S. A. J. Kimber, H. Mutka, T. Chatterji, T. Hofmann, P. F. Henry, H. N. Bordallo, D. N. Argyriou, and J. P. Attfield, Phys. Rev. B **84**, 104425 (2011).
[12] M. Lenertz, J. Alaria, D. Stoeffler, S. Colis, and A. Dinia, J. Phys. Chem. C **115**, 17190 (2011).
[13] X. Yao, J. Phys. Chem. A **116**, 2278 (2012).
[14] B. Kim, B. H. Kim, K. Kim, H. C. Choi, S.-Y. Park, Y. H. Jeong, and B. I. Min, Phys. Rev. B **85**, 220407 (2012).
[15] K. Singh, A. Maignan, D. Pelloquin, O. Perez, and C. Simon, J. Mater. Chem. **22**, 6436 (2012).
[16] R. Nakajima, J. Stöhr, and Y. U. Idzerda, Phys. Rev. B **59**, 6421 (1999).
[17] K. Koepernik and H. Eschrig, Phys. Rev. B **59**, 1743 (1999).
[18] M. Markkula, A. M. Arevalo-Lopez, and J. P. Attfield, J. Solid State Chem. **192**, 390 (2012).
[19] J. P. Perdew and Y. Wang, Phys. Rev. B **45**, 13244 (1992).
[20] F. de Groot, J. Electron Spectrosc. Relat. Phenom. **67**, 529 (1994).
[21] T. Burnus, Z. Hu, H. H. Hsieh, V. L. J. Joly, P. A. Joy, M. W. Haverkort, H. Wu, A. Tanaka, H.-J. Lin, C. T. Chen, and L. H. Tjeng, Phys. Rev. B **77**, 125124 (2008).
[22] B. T. Thole, P. Carra, F. Sette, and G. van der Laan, Phys. Rev. Lett. **68**, 1943 (1992).
[23] T_z is usually negligible in octahedral environment. In the simulations for the spectra, $T_z < 0.1\mu_B$.
[24] P. Carra, B. T. Thole, M. Altarelli, and X. Wang, Phys. Rev. Lett. **70**, 694 (1993).
[25] G. van der Laan and B. T. Thole, Phys. Rev. B **43**, 13401 (1991).
[26] See the Theo Thole Memorial Issue, J. Electron. Spectrosc. Relat. Phenom. **86**, 1 (1997).
[27] A. Tanaka and T. Jo, J. Phys. Soc. Jpn. **63**, 2788 (1994).

[28] $U_{dd} = 6.5$ eV, $U_{pd} = 8.2$ eV, and $\Delta = 6.5$ eV. Slater integrals were reduced by 70% from Hartree-Fock values.

[29] S. I. Csiszar, M. W. Haverkort, Z. Hu, A. Tanaka, H. H. Hsieh, H.-J. Lin, C. T. Chen, T. Hibma, and L. H. Tjeng, Phys. Rev. Lett. **95**, 187205 (2005).

[30] J. C. Slater and G. F. Koster, Phys. Rev. **94**, 1498 (1954).

[31] W. Harrison, *Electronic Structure and the Properties of Solids* (Dover, New York, 1989).

[32] S. V. Streltsov, A. S. Mylnikova, A. O. Shorikov, Z. V. Pchelkina, D. I. Khomskii, and V. I. Anisimov, Phys. Rev. B **71**, 245114 (2005).

[33] C. F. Chang, Z. Hu, H. Wu, T. Burnus, N. Hollmann, M. Benomar, T. Lorenz, A. Tanaka, H.-J. Lin, H. H. Hsieh, C. T. Chen, and L. H. Tjeng, Phys. Rev. Lett. **102**, 116401 (2009).

[34] H. Wu, C. F. Chang, O. Schumann, Z. Hu, J. C. Cezar, T. Burnus, N. Hollmann, N. B. Brookes, A. Tanaka, M. Braden, L. H. Tjeng, and D. I. Khomskii, Phys. Rev. B **84**, 155126 (2011).

[35] N. V. Smith, C. T. Chen, F. Sette, and L. F. Mattheiss, Phys. Rev. B **46**, 1023 (1992).

[36] N. Hollmann, Z. Hu, T. Willers, L. Bohatý, P. Becker, A. Tanaka, H. H. Hsieh, H.-J. Lin, C. T. Chen, and L. H. Tjeng, Phys. Rev. B **82**, 184429 (2010).

[37] J. van Elp, J. L. Wieland, H. Eskes, P. Kuiper, G. A. Sawatzky, F. M. F. de Groot, and T. S. Turner, Phys. Rev. B **44**, 6090 (1991).

[38] C. J. Ballhausen, *Introduction to Ligand Field Theory* (McGraw-Hill, New York, 1962).